EUROPEAN ORGANISATION FOR NUCLEAR RESEARCH (CERN)

Excess of charged over neutral K meson production in high-energy collisions of atomic nuclei

The NA61/SHINE Collaboration

Collisions of atomic nuclei at relativistic velocities produce new particles, predominantly mesons containing one valence quark and one valence anti-quark. These particles are produced in strong interactions, which preserve an approximate symmetry between up (u) and down (d) quarks. In the case of K meson production, if this symmetry were exact, it would result in equal numbers of charged (K^+ and K^-) and neutral (K^0 and $\overline{K}^0$) mesons in the final state. In this Letter, we report a measurement of the relative abundance of charged over neutral K meson production in collisions of argon and scandium nuclei at a center-of-mass energy of 11.9 GeV per nucleon pair. We find that production of K^+ and K^- mesons at mid-rapidity displays a significant excess of $(23.3 \pm 5.5)\%$ relative to that of the neutral K mesons. The origin of this unexpected excess remains to be elucidated.

Keywords: quarks, strong interaction, isospin symmetry, nucleus-nucleus collisions, strange meson production

arXiv:2312.06572v4 [nucl-ex] 6 Feb 2024

One of the main aims of basic research is the understanding of fundamental constituents and properties of matter, particularly the underlying fundamental interactions. Collisions of highly energetic atomic nuclei studied at large circular accelerators serve the specific purpose of understanding the short-range strong interaction occurring between the quarks, which build up the participating protons and neutrons.

At collision energies of several GeV (center-of-mass energy per nucleon pair) or more, it is generally assumed that the colliding nuclei form, on time scales of the order of 10^{-23} seconds, an intermediate system of deconfined quarks, anti-quarks and gluons characteristic of the early universe about 10^{-5} seconds after the Big Bang. Cooling down, this quark-gluon plasma ultimately "freezes out" into observable final state particles [1]. Studying these particle production phenomena is one of the main purposes of high-energy experiments located at CERN (Super Proton Synchrotron, Large Hadron Collider) and BNL (Relativistic Heavy Ion Collider).

These typically very abundant newly produced particles (hundreds or thousands per single nucleus-nucleus collision) are predominantly mesons containing one valence quark (q) and one valence anti-quark ($\overline{q}$). The most copiously produced are the up (u) and down (d) quarks, which also constitute protons and neutrons, but a large number of strange quarks (s), belonging to the second quark family of the standard model of particle physics is produced as well. The same is true for the corresponding anti-quarks: $\overline{u}$, $\overline{d}$, and $\overline{s}$.

The two colliding nuclei are made of protons and neutrons. These contain, respectively, (uud) and (udd) valence quarks. While initial-state valence quarks can also contribute to the production of new mesons, the dominant contribution to this process comes from creating new quark-anti-quark pairs. Generally, strong interactions are independent of quark type (flavor) in the limit of massless quarks. As such, exchanging the light u and d quarks (or $\overline{u}$ and $\overline{d}$ anti-quarks) should not significantly affect the result of the strong interaction. This feature is known as isospin symmetry. However, this symmetry does not apply to s quarks. Their production remains suppressed due to their significantly higher mass (the corresponding quark masses are $m_u = 2.16^{+0.49}_{-0.26}$ MeV, $m_d = 4.67^{+0.48}_{-0.17}$ MeV, and $m_s = 93.4^{+8.6}_{-3.4}$ MeV [2]). The same is valid for the heavy charm (c), beauty (b), and top (t) quarks, which all remain very strongly suppressed in nuclear collisions.[1]

Let us first consider the case when the two nuclei are made of an equal number of protons and neutrons (and therefore, also of an equal number of valence u and d quarks). Then, isospin symmetry implies that such collisions will result in closely equal abundances of u and d quarks and similarly, closely equal abundances of $\overline{u}$ and $\overline{d}$ anti-quarks.[2] This brings implications for particle production. It is commonly expected [5–9] that collisions of such "isospin-symmetric" nuclei will result in closely similar abundances of mesons of any particular type, for mesons containing u quarks and those containing d quarks. The same is expected for mesons containing $\overline{u}$ and $\overline{d}$ anti-quarks. A good example for this rule should be K mesons. With their masses differing by less than 1% ($m_{K^+} = m_{K^-} = 493.677 \pm 0.016$ MeV, $m_{K^0} = m_{\overline{K}^0} = 497.611 \pm 0.013$ MeV [2]), similar yields would be anticipated for the K^+ ($u\overline{s}$) and K^0 ($d\overline{s}$) states. Also, similar abundances would be expected for K^- ($s\overline{u}$) and $\overline{K}^0$ ($s\overline{d}$).

In the realistic case of nucleus-nucleus reactions studied experimentally, the two colliding nuclei are most often made of non-equal numbers of protons and neutrons. However, even for heavy nuclei with a significant excess of neutrons (*e.g.* Pb) the number of valence u and d quarks in the initial state of the reaction differs only by 14%. As a consequence, it is expected that in general, all types of high-energy

---

[1] Units in this Letter follow the Particle Data Group (PDG) [2] convention: masses and energies are expressed in MeV (or GeV), whereas momenta in MeV/c (or GeV/c). The relative differences are given as the ratio of the difference to the mean.

[2] With rare exceptions, nuclei with an equal number of protons and neutrons are in the ground state singlets of isospin [3]. A discussion of phenomenological aspects of the (approximate) isospin symmetry in particle production can be found in Ref. [4].

nucleus-nucleus collisions will bring similar abundances of u and d quarks, and also similar abundances of $\bar{u}$ and $\bar{d}$ anti-quarks in their final state. Correspondingly, one expects similar abundances for the produced mesons, and in particular, an approximate equality of charged and neutral K meson yields ($K^+ \approx K^0$, $K^- \approx \overline{K}^0$) is generally assumed. These expectations are supported by quantitative predictions of statistical models, which have been, up to now, very successful in the description of experimental data [10, 11].

In this Letter, we report a measurement of the relative abundance of charged (K^+, K^-) over neutral (K_S^0) meson production in the 10% most central collisions of argon (Ar) and scandium (Sc) nuclei, at center-of-mass energy per nucleon pair equal to $\sqrt{s_{NN}} = 11.9$ GeV. The Ar+Sc colliding system comprises 39 protons and 46 neutrons, which means that the corresponding number of u and d valence quarks differs by 5.5%. Notwithstanding, production of K^+ and K^- mesons displays an unexpected excess to that of the K_S^0 meson. The K_S^0 meson is a superposition of the two neutral states K^0 ($d\bar{s}$) and $\overline{K}^0$ ($s\bar{d}$), and its yield in the final state is equal to half of the summed production of these two states from the strong interaction.[3] The corresponding excess is quantified in terms of the ratio of yields of the produced K mesons:

$$R_K = \frac{K^+ + K^-}{K^0 + \overline{K}^0} = \frac{K^+ + K^-}{2K_S^0} \ . \tag{1}$$

This ratio remains above unity in the entire kinematic range available for measurement. Typically, the measured values exceed 1.2. Following our estimates, the observed surplus of production of K mesons containing u ($\bar{u}$) over these containing d ($\bar{d}$) quarks and anti-quarks corresponds to about four additional charged K particles per central Ar+Sc event.

Production of K mesons in central Ar+Sc collisions at the CERN SPS. The new experimental results presented in this Letter have been obtained by the NA61/SHINE fixed-target experiment at the CERN Super Proton Synchrotron [12]. The measurements of K^+ and K^- production in the 10% most central Ar+Sc reactions at $\sqrt{s_{NN}} = 11.9$ GeV have been published elsewhere [13]. This Letter presents the first measurement of K_S^0 production in nucleus-nucleus collisions from NA61/SHINE. Earlier data from this experiment, obtained for K_S^0 mesons in p+C, π^-+C, π^++C, π^++Be and p+p collisions can be found in Refs. [14–18].

The comparison of the rapidity distribution of K_S^0 mesons to the average of rapidity distributions for K^+ and K^- mesons is presented in Fig. 1. The rapidity y is a relativistic generalization of the particle's longitudinal velocity v_L, along the direction of the incoming nuclei: where c is the speed of light. In this Letter, we define rapidity in the collision center-of-mass system and positive y corresponds to the direction of the Ar nucleus.

In the entire range of rapidity covered by the measurement, the averaged charged K mesons prevail significantly over the neutral K_S^0 mesons. To quantify this effect, Table 1 presents the densities of K^+, K^- and K_S^0 production measured at mid-rapidity ($y \approx 0$). Here, the relative excess of charged mesons is $(23.3 \pm 5.5)\%$. Integration of the two distributions in Fig. 1 over positive rapidity, $y > 0$, gives 4.34 ± 0.07 and 3.22 ± 0.37 for the production rates per collision of $\frac{K^+ + K^-}{2}$ and K_S^0, respectively (total uncertainties are given; the quantities provided for charged K mesons are based on Ref. [13]). The resulting difference of 1.12 ± 0.38 corresponds to the surplus of charged (K^+ and K^-) over neutral (K^0 and $\overline{K}^0$) states equal

---

[3] The K^0 and $\overline{K}^0$ states are produced in strong interactions, but they decay through weak interactions. Consequently, in the final state, one observes linear combinations of the latter known as K^0 "short" (K_S^0) and K^0 "long" (K_L^0), where "short" and "long" refer to their weak decay lifetime. For more details, see Ref. [2].
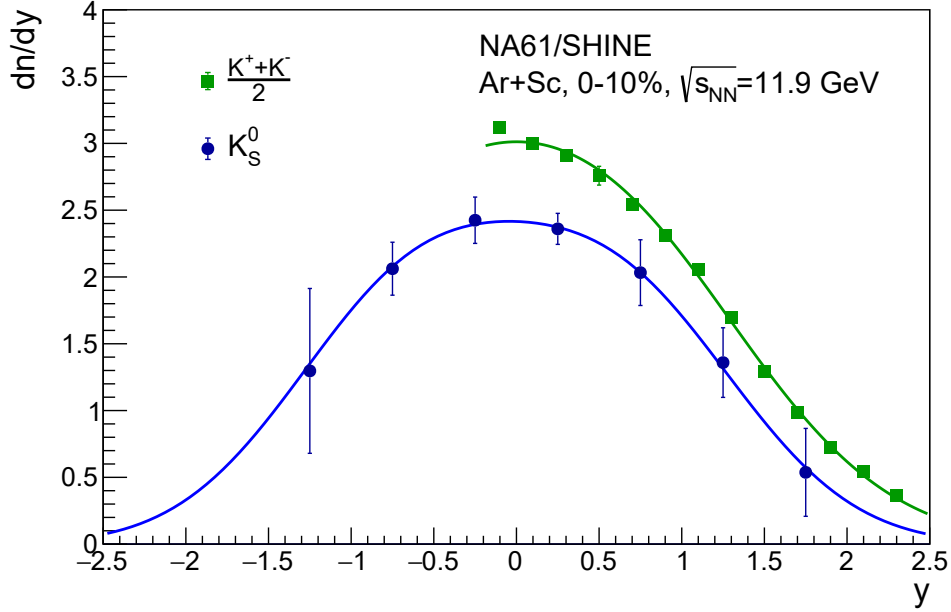
Figure 1: Comparison of rapidity spectrum of neutral (K_S^0) with the average spectrum of charged (K^+ and K^-) mesons. Total uncertainties, calculated as the square root of the sum of squared statistical and systematic uncertainties ($\sqrt{\text{stat}^2 + \text{sys}^2}$) are drawn. For charged K mesons, the total uncertainties were calculated separately for positively and negatively charged, and then propagated (typically, they remain below symbol size).

		statistical	systematic	total
$\left(\frac{dn}{dy}\right)_{y \approx 0}(K^+)$	3.949	$\pm\, 0.016$	$\pm\, 0.061$	$\pm\, 0.063$
$\left(\frac{dn}{dy}\right)_{y \approx 0}(K^-)$	2.053	$\pm\, 0.011$	$\pm\, 0.026$	$\pm\, 0.028$
$\left(\frac{dn}{dy}\right)_{y \approx 0}(K_S^0)$	2.433	$\pm\, 0.027$	$\pm\, 0.102$	$\pm\, 0.106$
charged-to-neutral K meson ratio: $R_K =$	1.233	$\pm\, 0.014$	$\pm\, 0.053$	$\pm\, 0.055$

Table 1: Densities of charged and neutral K mesons produced at mid-rapidity. The measurement was performed in the 10% most central Ar+Sc collisions at $\sqrt{s_{\text{NN}}} = 11.9$ GeV, as described in Methods. The excess of charged over neutral mesons is quantified by the ratio R_K defined in Eq. (1).

to 2.25 ± 0.76 at positive rapidity (proper rounding is taken). Under the assumption that the charged-to-neutral ratio would be similar also at negative rapidity, the total excess would amount to 4.5 ± 1.5 additional K^+ or K^- mesons per one central Ar+Sc collision.

A comparison of distributions of K^0_S with averaged K^+ and K^- mesons as a function of transverse momentum p_T (the momentum component perpendicular to the direction of the incoming nuclei) is shown in Fig. 2. Both distributions are integrated over the rapidity range $0 < y < 2$. The prevalence of charged over neutral K mesons is again evident. The insert in the figure shows the p_T-dependence of the ratio R_K. The corresponding excess of K mesons containing $u, \bar{u}$ over these containing $d, \bar{d}$ quarks and anti-quarks remains in the range 6–36% over the considered range of p_T.
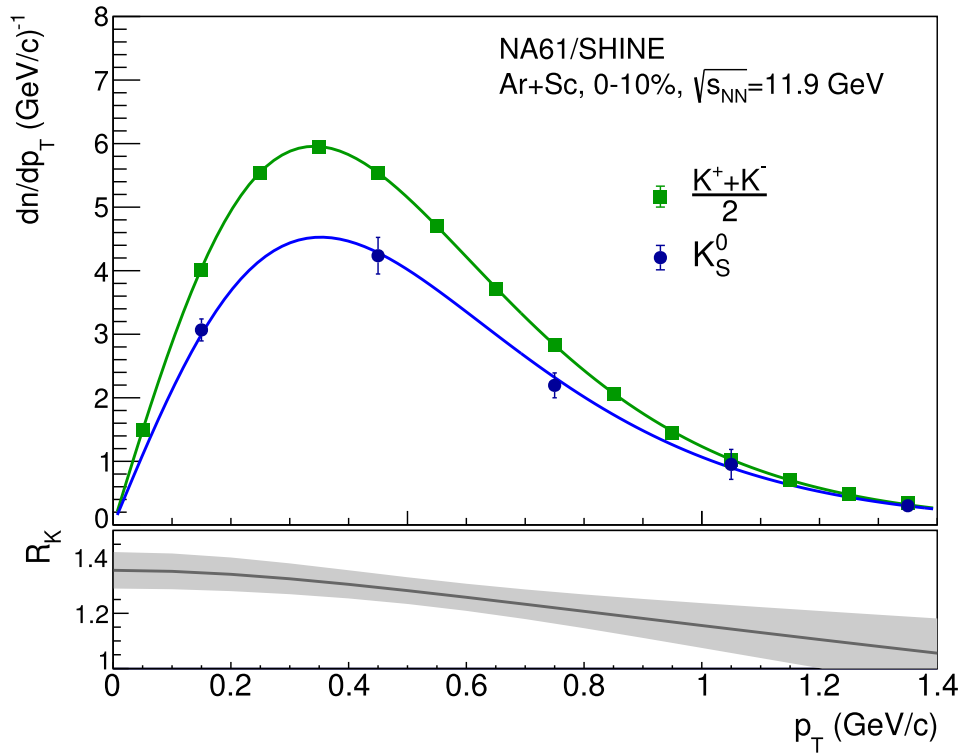
Figure 2: Comparison of transverse momentum spectrum of neutral (K^0_S) with the average spectrum of charged (K^+ and K^-) mesons. The bottom panel shows the ratio of the two distributions, as defined in Eq. (1). The meaning of the total uncertainties drawn is the same as in Fig. 1. For charged K mesons, the uncertainties remain below symbol size.
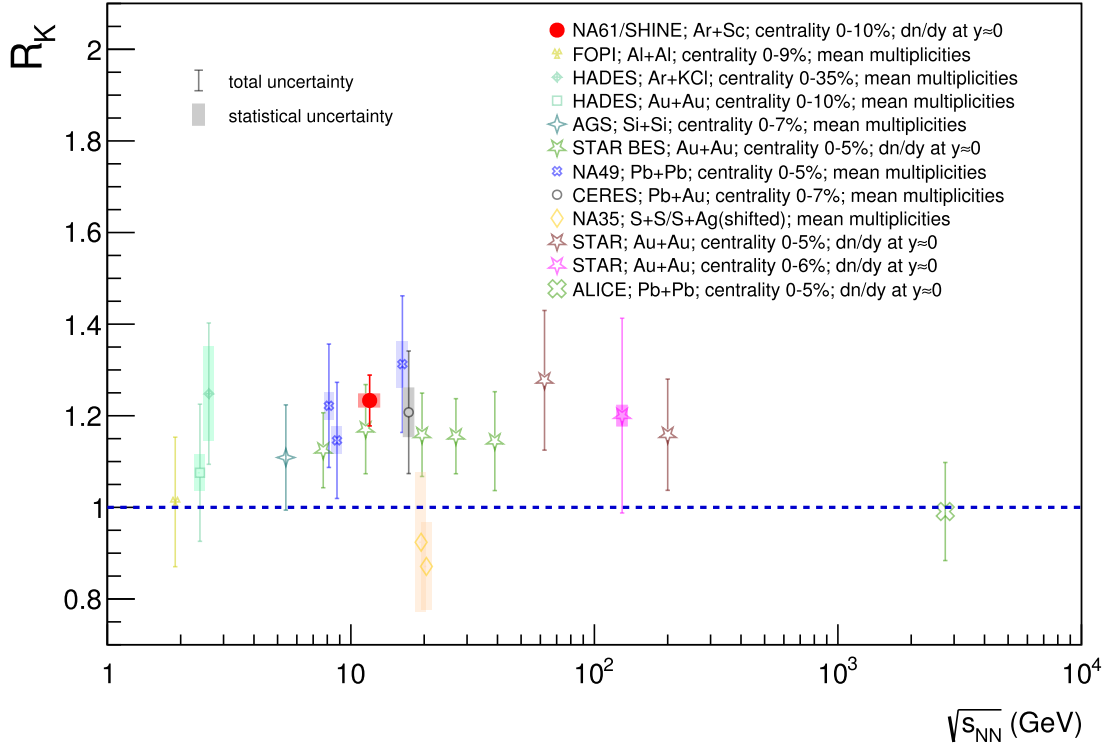
Figure 3: Ratio of charged to neutral *K* meson yields in nucleus-nucleus collisions as a function of collision energy. The measurement from NA61/SHINE is shown as a red dot. The remaining data points come from the compilation described in the text.

Comparison to previous experiments. Figure 3 shows the comparison between the present measurement of the ratio R_K at mid-rapidity, Table 1, and our compilation based on existing experimental results on $K^+ K^-$ and K^0_S production from the CERES [19], STAR BES [20, 21], STAR [22–25], ALICE [26, 27], NA35 [28–30], NA49 [31], HADES [32–35] and FOPI [36, 37] collaborations. We note that the latter compilation includes not only measurements at mid-rapidity, but also these of total multiplicities. This may increase the overall spread between the data points. We also note the sizeable uncertainties of the earlier measurements. These probably explain the fact that the aforementioned charged-over-neutral anomaly was never reported before as an experimental observation. Despite these uncertainties, a consistent picture emerges in the energy range $5 < \sqrt{s_{NN}} < 200$ GeV. With the unique exception of the NA35 experiment, all the data points correspond to an excess of charged over neutral *K* mesons. This excess may fade out at much higher energies, as suggested by ALICE data at $\sqrt{s_{NN}} = 2760$ GeV.

Discussion of the observed excess. It is to be remarked that given the prevalence of neutrons (*udd*) over protons (*uud*) in the two colliding nuclei, the contribution of valence quarks to *K* meson production would favour a small excess of *d* over *u* quarks. Consequently, it would bring the ratio R_K below unity, which is opposite to the observed result. Thus in this context, our observation remains an unexpected effect. At the same time, it goes against the expectations based on statistical models of particle production [10, 11].

A known effect of violation of equivalence of charged and neutral *K* states is the $\phi(1020)$ resonance,

which decays more often to charged (K^+K^-) than neutral ($K^0_S K^0_L$) mesons. However, the contribution of the $\phi(1020)$ to K meson production at NA61/SHINE energies is known from measurements performed in $p+p$ and Pb+Pb collisions [38–41]. The interpolation to the Ar+Sc system shows that this contribution is insufficient to explain the observed excess.

In summary, we have found an unexpected excess of charged over neutral K meson production in central Ar+Sc collisions at 11.9 GeV center-of-mass energy per nucleon pair. The experimental data show prevalence in production of K mesons containing u, $\overline{u}$ over these containing d, $\overline{d}$ quarks and anti-quarks, in the entire kinematic range available to the measurement. The measured excess corresponds to about two additional K^+ or K^- mesons produced at positive rapidity. Under reasonable assumptions, this gives about four additional charged K mesons per central Ar+Sc collision. At mid-rapidity, the relative excess of charged mesons is $(23.3 \pm 5.5)\%$. Although with large uncertainties, earlier data from other experiments in the collision energy range $5 < \sqrt{s_{NN}} < 200$ GeV are consistent with the present result.

The experimental results presented in this Letter are the subject of a theoretical analysis which is presented elsewhere [42]. This theoretical result indicates that the observed excess of charged K mesons is difficult to reconcile with current models. The origin of this unexpected excess remains to be elucidated.

Acknowledgments

References

[1] E. V. Shuryak, "Quantum Chromodynamics and the Theory of Superdense Matter," *Phys. Rept.* **61** (1980) 71–158.

[2] R. L. Workman *et al.*, [Particle Data Group Collab.], "Review of Particle Physics," *Prog. Theor. Exp. Phys.* **2022**, *083C01* (2022) .

[3] S. Lenzi and M. Bentley, *Test of Isospin Symmetry Along the N=Z Line. Lect. Notes Phys.* **764**, *57–98.* Springer Berlin Heidelberg, Berlin, Heidelberg, 2009.

[4] M. Gazdzicki and O. Hansen, "Hadron production in nucleon-nucleon collisions at 200-GeV/c: A Compilation," *Nucl. Phys. A* **528** (1991) 754–770.

[5] I. Shmushkevich, *Dokl. Akad. Nauk SSSR* **103** (1955) 235.

[6] N. Dushin and I. Shmushkevich, *Dokl. Akad. Nauk SSSR* **106** (1956) 801.

[7] A. J. MacFarlane, G. Pinski, and G. Sudarshan, "Shmushkevich's method for a charge independent theory," *Phys. Rev.* **140** (1965) B1045.

[8] C. G. Wohl, "Isospin Relations by Counting," *Am. J. Phys.* **50** (1982) 748–753.

[9] P.B. Pal, "An introductory course of particle physics," CRC Press, Taylor & Francis Group (2015).

[10] F. Becattini, M. Gazdzicki, A. Keranen, J. Manninen, and R. Stock, "Chemical equilibrium in nucleus-nucleus collisions at relativistic energies," *Phys. Rev. C* **69** (2004) 024905, `arXiv:hep-ph/0310049`.

[11] P. Braun-Munzinger, J. Stachel, J. P. Wessels, and N. Xu, "Thermal and hadrochemical equilibration in nucleus-nucleus collisions at the SPS," *Phys. Lett. B* **365** (1996) 1–6, `arXiv:nucl-th/9508020`.

[12] N. Abgrall *et al.*, [NA61/SHINE Collab.], "NA61/SHINE facility at the CERN SPS: beams and detector system," *J. Inst.* **9** (2014) P06005.

[13] H. Adhikary *et al.*, [NA61/SHINE Collab.], "Measurements of $\pi^{\pm}$, $K^{\pm}$, p and $\bar{p}$ spectra in ^{40}Ar+^{45}Sc collisions at 13A to 150A GeV/c," `arXiv:2308.16683 [nucl-ex]`.

[14] N. Abgrall *et al.*, [NA61/SHINE Collab.], "Measurements of $\pi^{\pm}$, $K^{\pm}$, K_S^0 , Λ and proton production in proton–carbon interactions at 31 GeV/c with the NA61/SHINE spectrometer at the CERN SPS," *Eur. Phys. J. C* **76** no. 2, (2016) 84, `arXiv:1510.02703 [hep-ex]`.

[15] H. Adhikary *et al.*, [NA61/SHINE Collab.], "Measurements of K_S^0, Λ, and $\overline{\Lambda}$ production in 120 GeV/c p+C interactions," *Phys. Rev. D* **107** no. 7, (2023) 072004, `arXiv:2211.00183 [hep-ex]`.

[16] H. Adhikary *et al.*, [NA61/SHINE Collab.], "Measurement of hadron production in π^{-}–C interactions at 158 and 350 GeV/c with NA61/SHINE at the CERN SPS," *Phys. Rev. D* **107** no. 6, (2023) 062004, `arXiv:2209.10561 [nucl-ex]`.

[17] A. Aduszkiewicz *et al.*, [NA61/SHINE Collab.], "Measurements of hadron production in π^{+}+C and π^{+}+Be interactions at 60 GeV/c," *Phys. Rev. D* **100** no. 11, (2019) 112004, `arXiv:1909.06294 [hep-ex]`.

[18] A. Acharya *et al.*, [NA61/SHINE Collab.], "K_S^0 meson production in inelastic *p+p* interactions at 158 GeV/*c* beam momentum measured by NA61/SHINE at the CERN SPS," *Eur. Phys. J. C* **82** no. 1, (2022) 96, arXiv:2106.07535 [hep-ex].

[19] M. Kalisky, *Reconstruction of charged kaons in the three pion decay channel in Pb+Au 158 AGeV collisions by the CERES experiment*. PhD thesis, Darmstadt, Tech. U., 2008. https://cds.cern.ch/record/1497739.

[20] J. Adam *et al.*, [STAR Collab.], "Strange hadron production in Au+Au collisions at $\sqrt{s_{NN}}$ = 7.7, 11.5, 19.6, 27, and 39 GeV," *Phys. Rev. C* **102** no. 3, (2020) 034909, arXiv:1906.03732 [nucl-ex].

[21] L. Adamczyk *et al.*, [STAR Collab.], "Bulk Properties of the Medium Produced in Relativistic Heavy-Ion Collisions from the Beam Energy Scan Program," *Phys. Rev. C* **96** no. 4, (2017) 044904, arXiv:1701.07065 [nucl-ex].

[22] C. Adler *et al.*, [STAR Collab.], "Kaon production and kaon to pion ratio in Au+Au collisions at $\sqrt{s_{NN}}$ = 130 GeV," *Phys. Lett. B* **595** (2004) 143–150, arXiv:nucl-ex/0206008.

[23] M. M. Aggarwal *et al.*, [STAR Collab.], "Strange and Multi-strange Particle Production in Au+Au Collisions at $\sqrt{s_{NN}}$ = 62.4 GeV," *Phys. Rev. C* **83** (2011) 024901, arXiv:1010.0142 [nucl-ex].

[24] G. Agakishiev *et al.*, [STAR Collab.], "Strangeness Enhancement in Cu+Cu and Au+Au Collisions at $\sqrt{s_{NN}}$ = 200 GeV," *Phys. Rev. Lett.* **108** (2012) 072301, arXiv:1107.2955 [nucl-ex].

[25] B. I. Abelev *et al.*, [STAR Collab.], "Systematic Measurements of Identified Particle Spectra in *pp*, *d*+Au and Au+Au Collisions at the STAR Detector," *Phys. Rev. C* **79** (2009) 034909, arXiv:0808.2041 [nucl-ex].

[26] B. B. Abelev *et al.*, [ALICE Collab.], "K_S^0 and Λ production in Pb-Pb collisions at $\sqrt{s_{NN}}$ = 2.76 TeV," *Phys. Rev. Lett.* **111** (2013) 222301, arXiv:1307.5530 [nucl-ex].

[27] B. Abelev *et al.*, [ALICE Collab.], "Centrality dependence of π, K, p production in Pb-Pb collisions at $\sqrt{s_{NN}}$ = 2.76 TeV," *Phys. Rev. C* **88** (2013) 044910, arXiv:1303.0737 [hep-ex].

[28] M. Gazdzicki and D. Rohrich, "Strangeness in nuclear collisions," *Z. Phys. C* **71** (1996) 55–64, arXiv:hep-ex/9607004.

[29] T. Alber *et al.*, [NA35 Collab.], "Strange particle production in nuclear collisions at 200 GeV per nucleon," *Z. Phys. C* **64** (1994) 195–207.

[30] J. Baechler *et al.*, [NA35 Collab.], "Production of charged kaons in proton - nucleus and nucleus-nucleus collisions at 200 GeV/nucleon," *Z. Phys. C* **58** (1993) 367–374.

[31] C. Strabel, "Energieabhangigkeit der K_S^0-Produktion in zentralen Pb+Pb Reaktionen." Diploma thesis, Johann Wolfgang Goethe-Universitat, 2006.

[32] J. Adamczewski-Musch *et al.*, [HADES Collab.], "Sub-threshold production of K_s^0 mesons and Λ hyperons in Au+Au collisions at $\sqrt{s_{NN}}$ = 2.4 GeV," *Phys. Lett. B* **793** (2019) 457–463, arXiv:1812.07304 [nucl-ex].

[33] J. Adamczewski-Musch *et al.*, [HADES Collab.], "Deep sub-threshold ϕ production in Au+Au collisions," *Phys. Lett. B* **778** (2018) 403–407, arXiv:1703.08418 [nucl-ex].

[34] G. Agakishiev *et al.*, [HADES Collab.], "ϕ decay: A relevant source for K$^-$ production at energies available at the GSI Schwerionen-Synchrotron (SIS)?," *Phys. Rev. C* **80** (2009) 025209, `arXiv:0902.3487 [nucl-ex]`.

[35] G. Agakishiev *et al.*, "In-Medium Effects on K^0 Mesons in Relativistic Heavy-Ion Collisions," *Phys. Rev. C* **82** (2010) 044907, `arXiv:1004.3881 [nucl-ex]`.

[36] P. Gasik *et al.*, [FOPI Collab.], "Strange meson production in Al+Al collisions at 1.9 A GeV," *Eur. Phys. J. A* **52** no. 6, (2016) 177, `arXiv:1512.06988 [nucl-ex]`.

[37] X. Lopez *et al.*, [FOPI Collab.], "Measurement of $K^*(892)^0$ and K^0 mesons in Al+Al collisions at 1.9A GeV," *Phys. Rev. C* **81** (2010) 061902, `arXiv:1006.1905 [nucl-ex]`.

[38] A. Aduszkiewicz *et al.*, [NA61/SHINE Collab.], "Measurement of ϕ meson production in $p+p$ interactions at 40, 80 and 158 GeV/c with the NA61/SHINE spectrometer at the CERN SPS," *Eur. Phys. J. C* **80** no. 3, (2020) 199, `arXiv:1908.04601 [nucl-ex]`.

[39] A. Aduszkiewicz *et al.*, [NA61/SHINE Collab.], "Measurements of $\pi^\pm$, K$^\pm$, p and $\bar{\text{p}}$ spectra in proton-proton interactions at 20, 31, 40, 80 and 158 GeV/c with the NA61/SHINE spectrometer at the CERN SPS," *Eur. Phys. J. C* **77** no. 10, (2017) 671, `arXiv:1705.02467 [nucl-ex]`.

[40] C. Alt *et al.*, [NA49 Collab.], "Energy dependence of ϕ meson production in central Pb+Pb collisions at $\sqrt{s_{\text{NN}}}$ = 6 to 17 GeV," *Phys. Rev. C* **78** (2008) 044907, `arXiv:0806.1937 [nucl-ex]`.

[41] S. V. Afanasiev *et al.*, [NA49 Collab.], "Energy dependence of pion and kaon production in central Pb+Pb collisions," *Phys. Rev. C* **66** (2002) 054902, `arXiv:nucl-ex/0205002`.

[42] W. Brylinski, M. Gazdzicki, F. Giacosa, M. Gorenstein, R. Poberezhnyuk, S. Samanta, and H. Stroebele, "Large isospin symmetry breaking in kaon production at high energies," `arXiv:2312.07176 [nucl-th]`.

[43] K. Werner, "The hadronic interaction model EPOS," *Nucl. Phys. Proc. Suppl.* **175-176** (2008) 81–87.

[44] R. Brun, R. Hagelberg, M. Hansroul, and J. C. Lassalle, "Simulation Program for Particle Physics Experiments, GEANT: User Guide and Reference Manual," tech. rep., CERN, Geneva, 1978. CERN-DD-78-2-REV, CERN-DD-78-2 `https://cds.cern.ch/record/118715`.

Methods

Experimental setup. The SPS Heavy Ion and Neutrino Experiment (SHINE) is a fixed-target detector operating at the CERN Super Proton Synchrotron (SPS). It is a multi-purpose spectrometer optimised to study hadron production in various collisions (hadron-proton, hadron-nucleus and nucleus-nucleus). The detection setup in its configuration used for the measurements reported here is described below. Its details and a description of the detector's performance can be found in Ref. [12].

The beamline is equipped with an array of beam detectors upstream and downstream of the target, used to identify and measure the trajectory of the beam particles and trigger the spectrometer data acquisition. The tracking devices of the NA61/SHINE spectrometer are Time Projection Chambers (TPCs). Two Vertex TPCs are placed inside a magnetic field. Two large-volume Main TPCs measure the charged particle trajectories downstream of the 4.5 Tm magnetic field. The latter provides the bending power for a precise determination of particle momenta. The information about the energy losses (dE/dx) of the charged particles in the TPCs, together with Time-of-Flight (ToF) measurements, allows for particle identification in a wide momentum range. The most downstream detector on the beamline is the Projectile Spectator Detector (PSD). It is used to measure the energy of the "spectator" remnant of the projectile nucleus, which is closely related to the collision centrality in nucleus-nucleus reactions.

Physics objects. This Letter compares the production of charged and neutral K mesons in Ar+Sc collisions at a center-of-mass energy per nucleon pair of 11.9 GeV. The $^{40}_{18}$Ar beam had a momentum of $75A\,\mathrm{GeV}/c$. The stationary target consisted of six $^{45}_{21}$Sc plates, with a total thickness of 6 mm.

A detailed account on the extraction of charged (K^+, K^-) yields can be found in Ref. [13]. Only the neutral K^0_S mesons are considered in the present analysis. They can be detected via their weak decay into two charged pions ($K^0_S \rightarrow \pi^+\pi^-$). The mean lifetime ($c\tau$) for this decay is 2.7 cm.

Analysis. Before the analysis of K^0_S mesons, the recorded Ar+Sc collision data undergo event and track selection procedures. Event selection uses information from the beam detectors to ensure the quality of the measured beam trajectory. It rejects events where more than one beam-target interaction occurred during the trigger-time window. It also reduces the background from off-target interactions based on information about the quality of the main interaction vertex. Finally, it selects the 10% most central collisions using the information from the PSD. This is realized by selection of the 10% lowest energy deposits from the spectator remnant of the Ar nucleus. The total number of recorded collisions (events) was $2.8 \cdot 10^6$, from which $1.1 \cdot 10^6$ (39%) remained after all cuts. For more details, especially the centrality selection, see Ref. [13].

The next step is the reconstruction of the charged particle tracks in the TPCs. Pattern recognition algorithms combine space points recorded in the TPCs into tracks. Their curvature and the magnetic field are used to compute the momenta of the corresponding particles. The minimum number of reconstructed space points in the VTPCs must be more than 10, and the computed momenta must be larger than $400\,\mathrm{MeV}/c$ (in the laboratory frame). The latter selection excludes a large fraction of low-momentum electrons from the analysis. The known positions of the target and the most probable intersection point of measured tracks defines the position of the primary vertex.

K^0_S reconstruction. Unlike the charged particles, the neutral K mesons do not leave a measurable track in the detectors. They are measured by reconstructing their oppositely charged decay products (daughter particles). The two-body decays of K^0_S create characteristic V-shaped particle pairs originating at the decay

vertex. This topology is called V^0. It is searched for with a dedicated V^0-finder algorithm that looks for track pairs of particles with opposite charges. These track pairs are extrapolated backwards until their mutual distance of closest approach is reached. If this distance is smaller than a given limit value, the track pair becomes a V^0 candidate with its origin at the decay vertex.

Two further cuts are placed on the track pairs. The first cut imposes a minimum value on the angle between the direction of the line joining the primary and decay vertices and the direction given by the vector sum of the momenta of the decay daughters. The second condition requires a minimum distance between the primary and decay vertex (a minimum length of the decaying particle). The corresponding cut requirements depend on K_S^0 rapidity, and are listed in Extended Data Table 2. Starting with the approximate decay point, a V^0-fitter program optimises the decay point position and the momenta of the decay daughters. Assuming that the daughter particles are pions, it is straightforward to reconstruct the invariant mass of the decaying particle (the invariant mass is defined as $m_{inv} = \sqrt{(\sum E_i)^2 - (\sum \overrightarrow{p_i})^2}$, where E_i are the energies of the decay products, $\overrightarrow{p_i}$ are their momenta, and $c \equiv 1$ is assumed).

The invariant mass distribution of V^0 candidates is populated by K_S^0 and Λ decays, photon conversion in some detector material, and spurious particle crossings. A K_S^0 signal will appear as a peak on a slowly varying background. For a double-differential K_S^0 analysis, the momentum space was divided into seven rapidity bins ranging from -1.5 to 2 and nine bins in transverse momentum from 0 to 2.7 GeV/c. The raw number of K_S^0 in a given kinematic bin is obtained from fits of appropriate signal and background functions to the invariant mass distribution of the corresponding V^0 candidates. The fitted signal function is taken as a Lorentzian and the background function is a third-order Chebychev polynomial. The integral of the signal function divided by the bin width is equal to the raw (uncorrected) number of the reconstructed K_S^0 in a given kinematic bin. Two typical invariant mass distributions with signal and background fits are shown in Extended Data Fig. 4.

Corrections. To correct the results for losses due to detection and data processing inefficiencies, detailed Monte Carlo simulations were performed. These simulations consisted of Ar+Sc collisions generated by the EPOS model [43] and particles propagated in the NA61/SHINE detector using the GEANT framework [44]. The charged particle tracks were reconstructed and analysed using the same software as used for the experimental data. The branching ratio of K_S^0 decays was considered in the GEANT framework. The final output of the simulation consisted of reconstructed K_S^0 multiplicities. The ratio of the number of K_S^0 simulated and reconstructed was used as a correction factor in each y–p_T bin.

Systematic uncertainties of the measured data points were estimated from the comparison of the results of the entire analysis (including Monte Carlo simulations and corrections) obtained with varying cut values. The reliability of the V^0 reconstruction and K_S^0 fitting procedures can be scrutinised by studying the K_S^0 lifetime. Extended Data Fig. 5 shows the computed mean lifetime of K_S^0 in seven rapidity bins. Good agreement with the average value provided by the PDG [2] is observed.

Transverse momentum distributions. The distributions shown in Extended Data Fig. 6 represent the final results of the K_S^0 analysis. The K_S^0 yields are shown as a function of transverse momentum in seven bins of rapidity. The data points are fitted with the function:

$$f(p_T) = A \cdot p_T \cdot \exp\left(-\frac{\sqrt{p_T^2 + m_0^2}}{T}\right), \tag{2}$$

in which A is a normalisation factor, T is the inverse slope parameter, and m_0 is the K_S^0 mass taken from Ref. [2]. The formula assumes $c \equiv 1$ for simplicity. The fit functions are plotted as red curves, and the inverse slope parameters obtained from the fits are reported in the figure's legend.

The transverse momentum distributions of charged and neutral K mesons drawn in Fig. 2 (of the main text) are also fitted with the function defined by Eq. (2). The bottom panel of the figure presents the ratio of the two fitted curves, with its uncertainty band obtained by propagation of the total uncertainties of the data points.

Rapidity distribution. The final K_S^0 yields in each bin of rapidity were obtained as the integrals of the curves fitted to the respective transverse momentum spectra, Eq. (2), including extrapolations to unmeasured regions. Comparison to the alternative method of replacing integrals in the measured regions by sums of data points brought only a negligible contribution to the systematic uncertainty. As apparent in Extended Data Fig. 6, extrapolations were needed only in the first and last rapidity bin. They amount to 88% and 6.2%, respectively. The large extrapolation in the first bin of rapidity results in the increase of the total uncertainty of the corresponding data point shown in Fig. 1 (of the main text). In this figure, the obtained rapidity distribution of the K_S^0 has been fitted with a function consisting of two Gaussians with centers displaced by a value of $\pm\Delta y$ with respect to $y = 0$. These Gaussians have the same widths but may have different amplitudes. The resulting small asymmetry of the fitted rapidity distribution originates from a combined effect of the mass asymmetry of the colliding target and projectile nuclei ($A_{\text{target}} = 45$ and $A_{\text{projectile}} = 40$) and the selection of central collisions by the energy measured in the kinematic region of the projectile spectator remnants. The former favours backward and the latter forward rapidities. The yields of charged K mesons at mid-rapidity listed in Table 1 (of the main text) were taken from Ref. [13]. They were determined in the interval $0.0 < y < 0.2$ as discussed therein. The yield of neutral K_S^0 mesons at mid-rapidity was determined at $y = 0$ from the aforementioned fit. Its systematic uncertainty was estimated the same way as for the data points (see above), and its statistical uncertainty was obtained by propagation of the statistical errors of the fit. Both statistical and systematic uncertainties of charged and neutral K yields were propagated into the ratio R_K. The additional uncertainty of R_K resulting from the difference in the mid-rapidity definition for charged and neutral mesons was estimated to be 0.5%, which is about 10% of the total systematic uncertainty.

Extended Data

	rapidity bin	$(-1.5, -1)$	$(-1, -0.5)$	$(-0.5, 0)$	$(0, 0.5)$	$(0.5, 1)$	$(1, 1.5)$	$(1.5, 2)$
cut value	cosine of angle	>0.999	>0.9995	>0.9995	>0.9995	>0.9995	>0.9999	>0.9999
	distance	>5 cm	>5 cm	>7.5 cm	>12.5 cm	>12.5 cm	>15 cm	>12.5 cm

Table 2: Track pair cuts. Values of the cuts on (top row) the cosine of the angle between the line joining the primary and decay vertex and the direction of the vector sum of decay daughter momenta, and (bottom row) the distance between the primary and decay vertex.
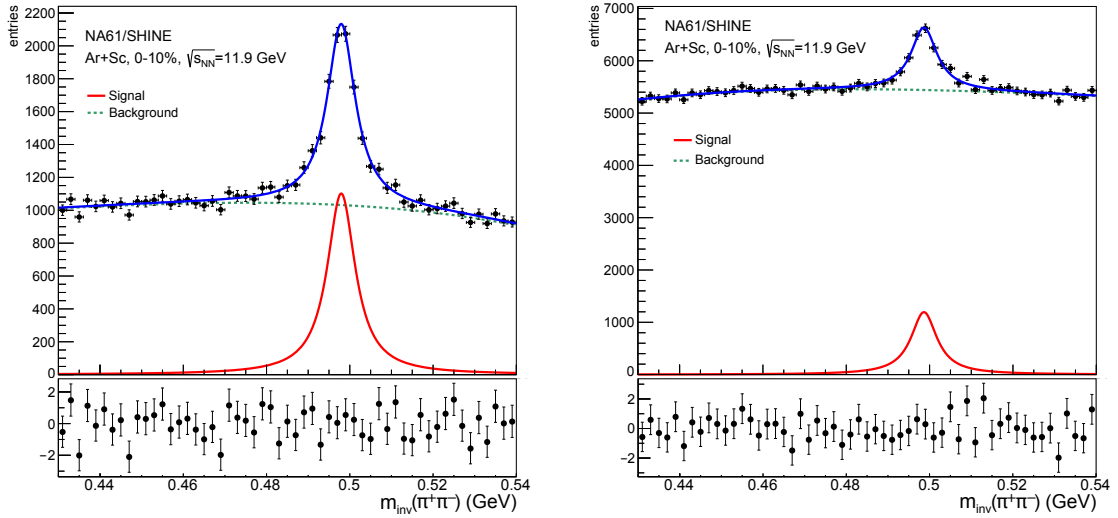
Figure 4: Examples of fitted invariant mass distributions. Two studied bins in rapidity y and transverse momentum p_T of the K_S^0 are presented, left: $y \in (-1.0, -0.5)$, $p_T \in (1.2, 1.5)$ GeV/c, right: $y \in (0.5, 1.0)$, $p_T \in (1.2, 1.5)$ GeV/c. The bottom panels show the difference between the experimental data and the fitted (Signal+Background) distribution, divided by the experimental uncertainty.

14
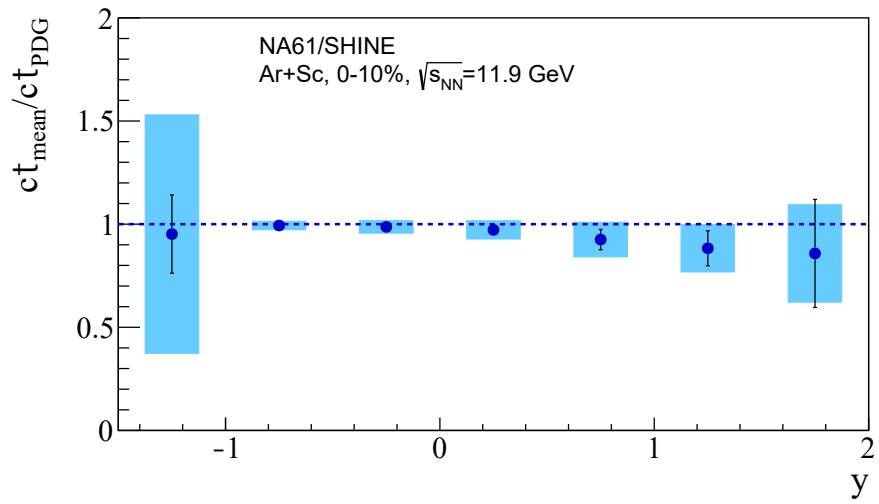
Figure 5: Mean lifetime of K^0_S mesons as a function of rapidity. The values obtained by NA61/SHINE are divided by the PDG value [2]. Statistical uncertainties are shown by vertical bars and systematic ones by shaded boxes.
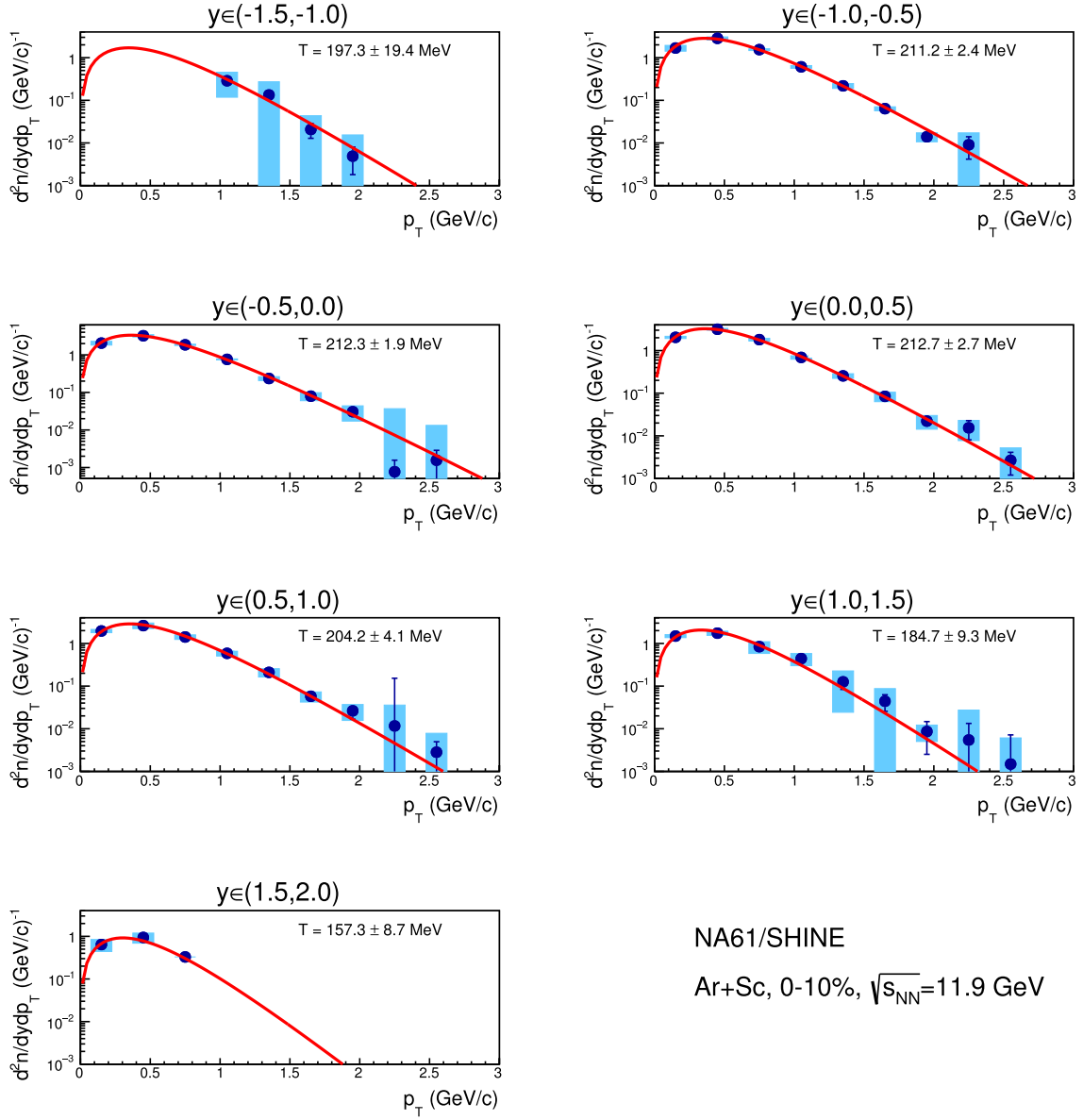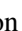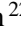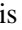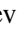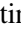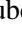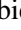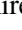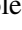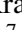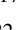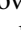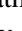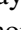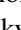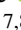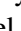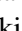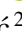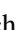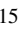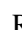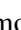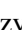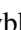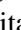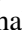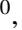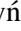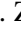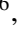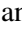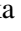
Figure 6: K_S^0 transverse momentum spectra in rapidity bins. Statistical uncertainties are shown by vertical bars and systematic ones by shaded boxes. Red curves represent fits of the data with the function defined in Eq. (2).

The NA61/SHINE Collaboration

H. Adhikary [13], P. Adrich [15], K.K. Allison [26], N. Amin [5], E.V. Andronov [22], I.-C. Arsene [12], M. Bajda [16], Y. Balkova [18], D. Battaglia [25], A. Bazgir [13], S. Bhosale [14], M. Bielewicz [15], A. Blondel [4], M. Bogomilov [2], Y. Bondar [13], A. Brandin [22], W. Bryliński [21], J. Brzychczyk [16], M. Buryakov [22], A.F. Camino [28], M. Ćirković [23], M. Csanád [8], J. Cybowska [21], T. Czopowicz [13], C. Dalmazzone [4], N. Davis [14], A. Dmitriev [22], P. von Doetinchem [27], W. Dominik [19], J. Dumarchez [4], R. Engel [5], G.A. Feofilov [22], L. Fields [25], Z. Fodor [7,20], M. Friend [9], M. Gaździcki [13], O. Golosov [22], V. Golovatyuk [22], M. Golubeva [22], K. Grebieszkow [21], F. Guber [22], S.N. Igolkin [22], S. Ilieva [2], A. Ivashkin [22], A. Izvestnyy [22], N. Kargin [22], N. Karpushkin [22], E. Kashirin [22], M. Kiełbowicz [14], V.A. Kireyeu [22], R. Kolesnikov [22], D. Kolev [2], Y. Koshio [10], V.N. Kovalenko [22], S. Kowalski [18], B. Kozłowski [21], A. Krasnoperov [22], W. Kucewicz [17], M. Kuchowicz [20], M. Kuich [19], A. Kurepin [22], A. László [7], M. Lewicki [20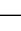], G. Lykasov [22], V.V. Lyubushkin [22], M. Maćkowiak-Pawłowska [21], Z. Majka [16], A. Makhnev [22], B. Maksiak [15], A.I. Malakhov [22], A. Marcinek [14], A.D. Marino [26], H.-J. Mathes [5], T. Matulewicz [19], V. Matveev [22], G.L. Melkumov [22], A. Merzlaya [12], Ł. Mik [17], S. Morozov [22], Y. Nagai [8], T. Nakadaira [9], M. Naskret [20], S. Nishimori [9], A. Olivier [25], V. Ozvenchuk [14], O. Panova [13], V. Paolone [28], O. Petukhov [22], I. Pidhurskyi [13], R. Płaneta [16], P. Podlaski [19], B.A. Popov [22,4], B. Pórfy [7,8], D.S. Prokhorova [22], D. Pszczel [15], S. Puławski [18], J. Puzović [23†], R. Renfordt [18], L. Ren [26], V.Z. Reyna Ortiz [13], D. Röhrich [11], E. Rondio [15], M. Roth [5], Ł. Rozpłochowski [14], B.T. Rumberger [26], M. Rumyantsev [22], A. Rustamov [1], M. Rybczynski [13], A. Rybicki [14], D. Rybka [15], K. Sakashita [9], K. Schmidt [18], A.Yu. Seryakov [22], P. Seyboth [13], U.A. Shah [13], Y. Shiraishi [10], A. Shukla [27], M. Słodkowski [21], P. Staszel [16], G. Stefanek [13], J. Stepaniak [15], M. Strikhanov [22], H. Ströbele [6], T. Šuša [3], Ł. Świderski [15], J. Szewiński [15], R. Szukiewicz [20], A. Taranenko [22], A. Tefelska [21], D. Tefelski [21], V. Tereshchenko [22], R. Tsenov [2], L. Turko [20], T.S. Tveter [12], M. Unger [5], M. Urbaniak [18], F.F. Valiev [22], D. Veberič [5], V.V. Vechernin [22], O. Vitiuk [20], V. Volkov [22], A. Wickremasinghe [24], K. Witek [17], K. Wójcik [18], O. Wyszyński [13], A. Zaitsev [22], E. Zherebtsova [20], E.D. Zimmerman [26], A. Zviagina [22], and R. Zwaska [24]

---

† *deceased*

1 National Nuclear Research Center, Baku, Azerbaijan

2 Faculty of Physics, University of Sofia, Sofia, Bulgaria

3 Ruđer Bošković Institute, Zagreb, Croatia

4 LPNHE, Sorbonne University, CNRS/IN2P3, Paris, France

5 Karlsruhe Institute of Technology, Karlsruhe, Germany

6 University of Frankfurt, Frankfurt, Germany

7 HUN-REN Wigner Research Centre for Physics, Budapest, Hungary

8 Eötvös Loránd University, Budapest, Hungary

9 Institute for Particle and Nuclear Studies, Tsukuba, Japan

10 Okayama University, Japan

11 University of Bergen, Bergen, Norway

12 University of Oslo, Oslo, Norway

13 Jan Kochanowski University, Kielce, Poland

14 Institute of Nuclear Physics, Polish Academy of Sciences, Cracow, Poland

15 National Centre for Nuclear Research, Warsaw, Poland

16 Jagiellonian University, Cracow, Poland

[17] AGH - University of Science and Technology, Cracow, Poland

[18] University of Silesia, Katowice, Poland

[19] University of Warsaw, Warsaw, Poland

[20] University of Wrocław, Wrocław, Poland

[21] Warsaw University of Technology, Warsaw, Poland

[22] Affiliated with an institution covered by a cooperation agreement with CERN

[23] University of Belgrade, Belgrade, Serbia

[24] Fermilab, Batavia, USA

[25] University of Notre Dame, Notre Dame, USA

[26] University of Colorado, Boulder, USA

[27] University of Hawaii at Manoa, Honolulu, USA

[28] University of Pittsburgh, Pittsburgh, USA